18th International Conference on Structural Mechanics in Reactor Technology (SMiRT 18)
Beijing, China, August 7-12, 2005
SMiRT18-G08-3

LOAD BEARING CAPACITY OF DEGRADED NUCLEAR PIPING

E. Roos, K.-H. Herter, X. Schuler
MPA, University of Stuttgart, Pfaffenwaldring 32, D-70569 Stuttgart, Germany
Phone: +49 711 685 2601, Fax: +49 711 685 3053
E-mail: xaver.schuler@mpa.uni-stuttgart.de

J. Chattopadhyay, B.K. Dutta, H.S. Kushwaha
Bhabha Atomic Research Centre (BARC), RSD, Hall-7, Mumbai – 400085, India
E-mail: jchatt@apsara.barc.ernet.in

ABSTRACT

Integrity assessment of piping components with postulated cracks is important for safe and reliable operation of power plants. While various equations and methods are available for prediction of the load bearing capacity of pipes and elbows, it is very important to choose the correct equation and method whose predictions are consistent, safe but not too conservative with respect to the experimental results. Towards this goal, a comprehensive *Component Integrity Assessment Program* was initiated under a joint MPA-BARC collaborative program where a large number of austenitic and ferritic pipes and elbows of nominal diameter of 50 – 400 mm with various crack configurations and sizes were tested. These test results along with results of previous tests were analysed with various available limit load equations present and also with the R6 method. Based on the comparison of these test results and predictions, the correct equation and method are recommended to reliably predict the load bearing capacity of flawed pipes and elbows reliably.

Keywords: Integrity assessment, piping, leak-before-break (LBB) behaviour, analytical/numerical and experimental investigations, engineering and fracture mechanics methods, limit load calculations

1. INTRODUCTION

The investigation of the failure behaviour of pipes has been an evolutionary process that was initiated from the gas and oil industry to understand large breaks occurring in pipeline systems. The main work in piping systems started about 1950. Since that time numerous investigations in the experimental and numerical field were performed so that the failure behaviour and failure load of pipes could be well assessed and hence the safety margin also. With the start of operation of commercial nuclear power plants there was an additional need for tools to assess reliably the failure behaviour of piping systems under different loading and environmental conditions.

In all countries, power plants are designed, constructed and operated on the basis of safety criteria, guidelines and technical codes, for example ASME (2001). There are requirements also for nuclear power plants to take into account not only the stresses resulting from operating loads but also the impacts of accidents upon the integrity of pressurized components. Such accident considerations include extreme loads, for example, earthquake and postulated pipe failure. For these loading conditions it must be demonstrated that either catastrophic failures can be excluded or, otherwise, that resultant consequential damage will not lead to critical accident sequences. This is the object of the integrity concept. Therefore, it is very important that the analytical calculation methods for integrity assessment of degraded piping components are properly validated with respect to experimental results. Towards this goal, fracture tests have been carried out on cracked piping components made of ferritic and austenitic steel under various loading combination of internal pressure and bending moment. These test results have been further analysed by various analytical methods, e.g. plastic limit load (PLL), R6 method, etc. This paper describes the experimental procedure, test results and analysis.

2. METHODS TO PROVE INTEGRITY OF PIPING COMPONENTS

There are various analytical methods, e.g. plastic limit load, R6 method, etc., to assess the integrity of piping components with cracks subjected to static loads. These methods are briefly described below.

2.1 Plastic Limit Load

For small size piping components or pipes made of very tough material, the role of fracture mechanics in assessment of integrity may not be significant. This is because the plastic zone near the crack tip engulfs the entire tensile ligament before the crack driving force exceeds the material fracture toughness. For these cases, the plastic limit load governs the load bearing capacity of the component rather than the unstable fracture load. There are various plastic limit load formulae for piping components. The plastic limit moment of a through-wall circumferentially cracked pipe subjected to bending moment is calculated as follows (Kanninen et al,1982) :

$$M_L = 4R^2 t\sigma_f [\cos(\theta/2) - 0.5 \sin(\theta)] \quad (1)$$

where, R is the mean radius of the pipe cross section, t is the wall thickness, σ_f is the pipe material flow stress taken as the average of yield and ultimate stress i.e. $\sigma_f=0.5(\sigma_y+\sigma_u)$ and θ is the semi-crack angle. Kastner et al (1981) have observed that the choice of flow stress has a great influence in the estimation of critical crack lengths (and hence the critical moments also), especially for large crack size. While using $\sigma_f=(\sigma_y+\sigma_u)/2.4$ for axially cracked pipes under internal pressure, Kastner et al obtained all the experimental results conservatively with respect to the theoretical predictions. Moulin and Delliou (1996) also suggest a reduction factor of '0.85' to Eq. (1) to account for crack propagation at maximum moment. This is comparable to the definition of $\sigma_f=(\sigma_y+\sigma_u)/2.4$ instead of $\sigma_f=(\sigma_y+\sigma_u)/2$ in Eq. (1). For a conservative estimate of limit load, one can set the flow stress equal to the yield stress i.e. $\sigma_f=\sigma_y$ in Eq. (1).

In the case of combined internal pressure and bending moment, the plastic collapse moment is given as (Kanninen et al, 1982):

$$M_L = 4R^2 t\sigma_f [2\cos(\alpha/2) - 0.5 \sin(\theta)] \quad (2)$$

with

$$\alpha = 0.5\theta + (p\pi R_i^2)/(4Rt\sigma_f) \quad (3)$$

where p is the internal pressure and R_i is the internal radius of the pipe.

For an elbow with a through-wall circumferential crack under in-plane bending moment, the limit moment is given by Zahoor (1990), Miller (1988) and very recently by Chattopadhyay et al (2004). Zahoor (1990) and Miller (1988) do not differentiate between closing and opening mode of bending moment. However, it is well known that deformation characteristics of elbow under these two bending modes are distinctly different. Considering this aspect, Chattopadhyay et al (2004) give separate limit moment formulae for closing and opening moments. The limit moment equation given by Zahoor (1990) is :

$$M_L = M_o\left[1 - 0.2137\left(\frac{a}{D}\right) - 0.0485\left(\frac{a}{D}\right)^2 - 10559\left(\frac{a}{D}\right)^3\right] \quad (4)$$

$$M_o = 0.935\sigma_f D^2 t h^{2/3} \quad (5)$$

The range of applicability is $a/D \le 0.8$, $h=4R_b t/D^2 \le 0.5$ and $D/t \ge 15$, where, a is the half crack length, D is the mean diameter of the elbow cross section, R_b is the mean bend radius of the elbow, t is the elbow wall thickness, $h=4R_b t/D^2$ is the elbow factor and σ_f is the material flow stress, usually taken as the average of yield and ultimate strengths.

The limit moment equation given by Miller (1988) is as follows:

$$M_L = M_o [\ 1.0 - 1.5(\theta/\pi)] \quad (6)$$

where, M_o is as defined in Eq. (5) and θ is the semi-circumferential crack angle.

The limit moment according to Chattopadhyay et al (2004) is as follows:

Closing mode

$$M_L = M_o X \quad (7)$$

$$M_0 = 1.075\, h^{2/3}\, (4R^2 t\sigma_y) \quad (8)$$

The function *X* is shown in Table 1.

Table 1 A_o, A_1 and A_2 values for function $X=A_o+A_1(\theta/\pi)+A_2(\theta/\pi)^2$

R/t	A_o	A_1	A_2	θ limits
5	1.1194	-0.7236	-2.0806	for $45^o \le 2\theta \le 150^o$ and *X* = 1for $2\theta < 45^o$
7.5	1.1185	-0.3420	-2.5200	for $60^o \le 2\theta \le 150^o$ and *X* = 1 for $2\theta < 60^o$
10	0.9655	1.0152	-4.6800	for $60^o \le 2\theta \le 150^o$ and *X* = 1 for $2\theta < 60^o$
15	1.1400	0.3000	-3.6000	for $90^o \le 2\theta \le 150^o$ and *X* = 1 for $2\theta < 90^o$
20	0.6400	3.4200	-7.920	for $90^o \le 2\theta \le 150^o$ and *X* = 1 for $2\theta < 90^o$

Opening mode

Same form as Eq. (7) used for $5 \le R/t \le 20$ with M_o and *X* given as follows :

$$M_0 = (1.0485\, h^{1/3} - 0.0617)\, (4R^2 t\sigma_y) \quad (9)$$

$$X = 1.127 - 1.8108\left(\frac{\theta}{\pi}\right) \qquad \text{or } 45^o \le 2\theta \le 150^o \quad (10)$$

$$= 1 - 0.8\left(\frac{\theta}{\pi}\right) \qquad \text{or } 0^o \le 2\theta \le 45^o$$

The limit moment for a short radius elbow ($R_b/D=1$) with an axial through wall crack at the crown is given by Zahoor (1990) as follows :

$$M_L = M_o\left[1 - 0.15\left(\frac{a}{D}\right)\right] \quad (11)$$

M_o is as defined in Eq. (5). The range of applicability is: $a/D \le 0.9$, $h = 4R_b t/D^2 \le 0.5$ and $D/t \ge 15$

2.2 R6 Approach

The R6-Method is based on the idea that, depending on the materials condition, failure of a component can take any form from brittle fracture to fully plastic deformation with the transition between the two extreme points being assumed to be continuous.

The limit curve was defined as follows:

$$K_r = (1 - 0.14\, L_r^2)\, (0.3 + 0.7\exp.(-0.65\, L_r^6)) \quad (12)$$

and

$$L_r(\max) = \sigma_f / \sigma_y \text{ and } \sigma_f = (\sigma_y + \sigma_f)/2 \quad (13)$$

The loading parameters of the pipe are given by $L_r = F/F_{collapse}$ as ratio of actual load F to plastic limit load $F_{collapse}$ and $K_r = K_I/K_{Ic} = \sqrt{J/J_i}$ as ratio of actual stress intensity factor K_I as a function of crack size and the fracture mechanics material characteristic K_{Ic} for linear-elastic and J_i for elastic-plastic conditions (Milne et al, 1986).

In the above equation, J is derived from the linear elastic K_I value. According to this concept, the onset of stable crack extension occurs when the load point formed by L_r and K_r is on the limit curve. Instability is derived from the load path, which forms a tangent to the limit curve, taking into consideration stable crack extension. A schematic diagram of the application of this procedure is shown in Figure 1. For this purpose, the constant load F acting in L_r is normalized by the crack-length-dependent limit load $F_{collapse}(a+\Delta a)$. The normalization of K_I, for example, for the applied J-integral, is carried out according to $J=J(a+\Delta a)$ with the likewise crack-length-dependent K_{Ic} curve ($J_R(\Delta a)$) being used as a material characteristic, taking into account also the crack extension. However, for this procedure, it is important that piping component should have the same or less stress triaxiality (constraint) in the ligament of the cracked section compared to that of the fracture mechanics specimens.

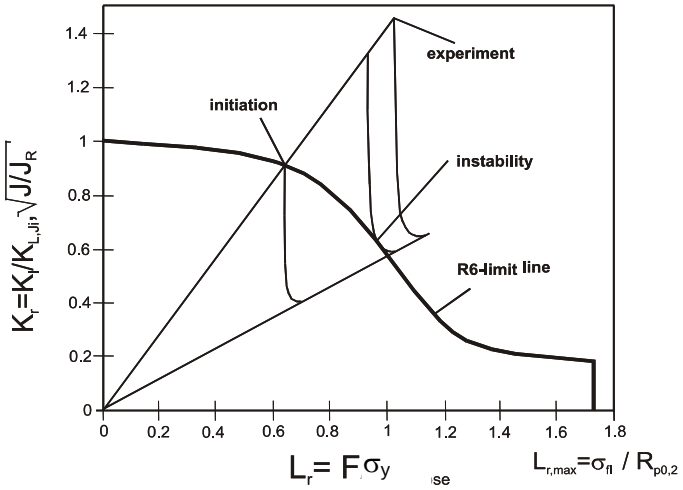

Fig. 1 Application of the R6 method

3. FRACTURE TESTS ON PIPING COMPONENTS

To validate various analytical methods for integrity assessment of degraded piping components as described above, a number of fracture tests have been carried out on pre-cracked pipes and elbows made of ferritic and austenitic steel under the comprehensive *Component Integrity Test Program* (Chattopadhyay et al, 2000, Chattopadhyay et al, 2005, Roos et al, 2000). These are described briefly in the following paragraphs.

3.1 Test Boundary Conditions

3.1.1 Material

The pipes of nominal diameters DN50, DN80 and DN300 were fabricated of the austenitic material X 10 CrNiNb 18 9 and those of nominal diameter DN200 from the material X 10 CrNiTi 18 9. In addition pipes and elbows of nominal diameters DN200 and DN400 were fabricated of the ferritic material SA333Gr6. The characteristic strength, ductility and fracture mechanics properties were determined as shown in Table 2. All the values are higher than the requirements given in the nuclear safety standards.

Table 2 Material properties

Pipe/ Elbow	Material	Yield Strength (0.2% proof stress) σ_y (MPa)	Ultimate Tensile Strength σ_u (MPa)	Young's Modulus E (MPa)	Reduction of Area Z (%)	Elongation A5 (%)	J_i (stretched zone) (N/mm)
DN400	SA333Gr6						
	Base metal	312	459	203000	70	41	236
DN300	X 10CrNiNb 18 9						
	Base metal	253	577	197 000	71	61	213-361
	Weld metal	442	635	170 500	52	37	80-117
DN200	X 10CrNiTi 18 9						
	Base metal	227	579	197 800	78	60	302-398
	Weld metal	467	695	196 600	48	35	73-146
DN200	SA333Gr6						
	Base metal	288	420	203000	70	36	220
DN80	X 10CrNiNb 18 9						
	Base metal	259	619	198 500	80	58	229-258
	Weld metal						288-317
DN50	X 10CrNiNb 18 9						
	Base metal	260	636	191 300	78	56	229-258
	Weld metal						288-317

3.1.2 Test Specimens and Set up

Test specimens consisted of pipes or elbows with through-wall or part-through circumferential cracks under combined internal pressure and bending moment or in some cases pure bending moment. Figures 2a and 2b show the crack configurations in the elbows. In the case of elbows, straight pipes of length 400-600 mm were welded on either side to allow free ovalisation of the elbow cross section. All the specimens were fatigue pre-

cracked by remote loading. Loading of the austenitic test pipes was achieved by internal pressure and a superimposed external bending moment using bending rigs specially made for these tests, Figure 3. The bending moment was introduced into the test pipe through a lever arm and extension pipes by means of two double acting (push-pull) hydraulic cylinders. In the case of ferritic pipes, moment loading was applied through the four point bending arrangement shown in Figure 4. In the case of elbows, the loading arrangement is shown in Figure 5. The moment loading was applied quasi-statically in all cases. Tables 3 and 4 give the details of the test specimens.

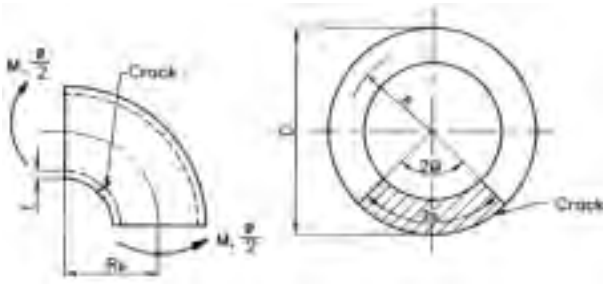

Fig. 2a. Sketch of elbow with through wall circumferential crack at the intrados

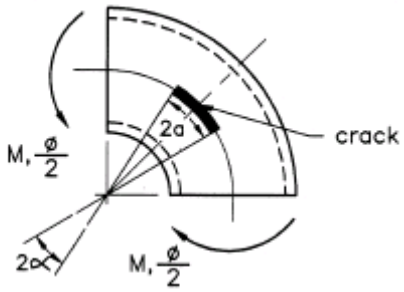

Fig. 2b Sketch of elbow with through wall axial crack at the crown

3.2 Test Results

3.2.1 Austenitic pipes

Load Bearing and Deformation Behaviour

A characteristic feature for the description of the overall behavior is the applied loading plotted against the deformation (e.g. pipe bend angle). The high capacity for deformation of all pipes (with and without cracks) could be demonstrated. All the test pipes could be loaded up to the attainment of the maximum possible bend angle limited by the bending rig or beyond the maximum loading (peak load) of the test pipes without the occurrence of failure in the form of massive fracture (no unstable crack extension). The collapse load determined in accordance with ASME III. App. II-1430 was clearly exceeded in all the tests. The strain measurements showed the bending moment introduced was practically constant along the pipe axis and agreed with the moment determined from the hydraulic cylinder pressure.

Table 3 Test matrix of pipes

Pipe Dimensions			Material	Crack		Internal pressure (MPa)	Four point bending loading span (mm)	
Nominal Diameter	OD (mm)	Thickness (mm)		Depth (a/t)	Angle 2θ (^{o})		Outer	Inner
DN400	406	32.3	SA333Gr6	1.0	96 – 158	0	5820	1480
DN300	331	32.1	X 10 CrNiNb 18 9	0.5 – 1.0	60 – 120	16	-	-
DN200	219.1	14.2	X 10 CrNiTi 18 9	0.5 – 1.0	120 – 270	7	-	-
DN200	219	15.1	SA333Gr6	1.0	66 – 157	0	4000	1480
DN80	88.9	8.8	X 10 CrNiNb 18 9	0.25 – 1.0	60 – 120	16	-	-
DN50	60.3	8.8	X 10 CrNiNb 18 9	0.25 – 1.0	60 – 120	16	-	-

As compared with the behaviour of un-cracked pipes, cracks of depth up to a/t=0.75 (t - wall thickness, a - crack depth) and circumferential extent 2θ up to 120^O (θ - half the crack circumferential angle) in the DN50 and DN80 pipes, of depth up to a/t=1.0 and circumferential extent 2θ up to 60^o in the DN200 pipes and of depths up to a/t=0.5 and circumferential extent 2θ up to 120^o in the DN300 pipes merely caused a small reduction in the overall load bearing capacity. Depending on the pipe and crack geometry, in the majority of the tests conducted the bending moment could be raised increasingly up to the maximum pipe bend angle so that by the end of the

tests the maximum load bearing capacity had still not been reached as is shown for example in Figures 6 to 8 for tests on pipes of DN300, DN200 and DN80 mm nominal diameter.

Fig. 3 Photograph of fracture test set-up of austenitic pipe

Fig. 5 Photograph of fracture test set-up of elbow

Fig. 4 Photograph of fracture test set-up of ferritic pipe under four point bending load

Failure Behaviour

Crack initiation took place each time clearly before the theoretical collapse load or before the maximum loading attained in the test. Crack initiation was determined by potential probe measurements and photographic records.

- Pipes of DN50 nominal diameter (austenitic material): In tests with defect dimensions a/t=0.25 with $2\theta=120^{O}$ and a/t=0.75 with $2\theta=60^{O}$ no crack initiation could be determined. In the remaining tests even with circumferential slits (a/t=1) only slight stable crack growth occurred.
- Pipes of DN80 nominal diameter (austenitic material): In tests with defect dimensions a/t=0.25 with $2\theta=120^{O}$ no crack initiation could be determined. In the remaining tests even with a circumferential through-wall crack (a/t=1) only stable crack growth occurred.
- Pipes of DN200 and DN300 nominal diameter (austenitic material): Stable crack growth occurred at times following crack initiation. At no time were indications of unstable crack propagation present.

Table 4 Test matrix of elbows

Test reference number	R_b (mm)	Outer dia. (mm)	t_{av} (mm)	Moment arm length* (mm)	Crack orientation	Crack location	Bending mode	Crack angles after fatigue pre-crack (2θ)
ELTWIN8-1	207	219	19.1	825.72	Circumferen.	Intrados	Opening	94.96^{o}
ELTWIN8-2	207	219	18.8	825.72	Circumferen.	Intrados	Opening	125.16^{o}
ELTWEX8-4	207	219	19.3	825.72	Circumferen.	Extrados	Closing	98.24^{o}
ELTWEX8-6	207	219	19.0	825.72	Axial	Crown	Closing	2a=109.2 mm
ELTWIN16-1	609	406	36.4	840.22	Circumferen.	Intrados	Opening	95.89^{o}
ELTWIN16-2	609	406	36.8	840.22	Circumferen.	Intrados	Opening	122.79^{o}
ELTWEX16-3	609	406	35.1	840.22	Circumferen.	Extrados	Closing	64.85^{o}
ELTWEX16-4	609	406	35.7	840.22	Circumferen.	Extrados	Closing	94.11^{o}
ELTWEX16-5	609	406	37.6	840.22	Circumferen.	Extrados	Closing	124.0^{o}
ELTWCR16-6	609	406	36.2	840.22	Axial	Crown	Opening	2a=210 mm

*Moment arm length is the perpendicular distance between the loading line and mid-section of elbow center-line for conversion of load to moment

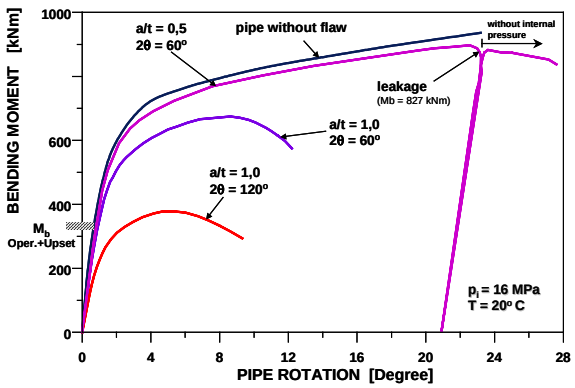

Fig. 6 Load bearing behaviour of austen- itic pipes with nominal diameter DN300 (OD 331 mm, t=32 mm) and internal pressure 16 MPa at room temperature

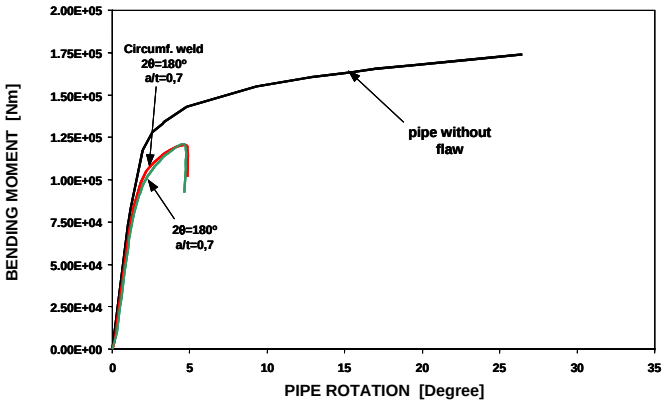

Fig. 7 Load bearing behaviour of austen- itic pipes with nominal diameter DN200 and internal pressure 7 MPa at room temperature

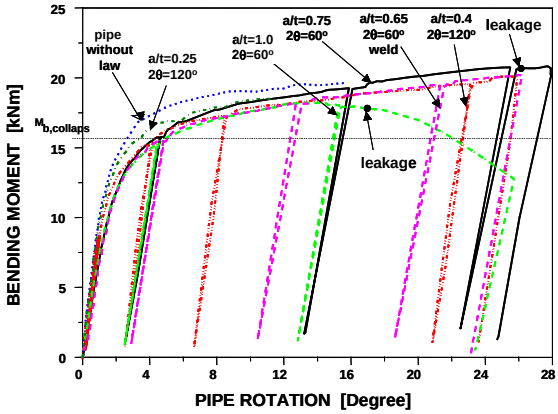

Fig. 8 Load bearing behaviour of austenitic pipes with nominal diameter DN80

In none of the tests carried out did a failure in the form of a massive fracture (large break) occur (no unstable crack propagation observed). Depending on the initial crack size and the pipe dimensions, no or only slight stable crack growth occurred (e.g. in DN50 and DN80 with defect dimensions a/t=0.25 and $2\theta=120^{O}$) ranging up to pronounced stable crack growth (e.g. in DN200 and DN300 with defect dimensions equal to or greater than a/t=0.5 and $2\theta=120^{O}$). In the tests in which the maximum load was attained, in all cases stable crack extension occurred up to the maximum load after crack initiation. Even after passing beyond the maximum load no unstable crack behaviour appeared. Therefore, in the tests carried out up to leakage, leak-before-break behaviour could be proven under the given loading conditions.

3.2.2 Ferritic Pipes

Pipe fracture test results are expressed in the form of load vs. load-line-displacement of the four point bending arrangement and load vs. crack growth curves. Crack growth has been measured by an image processing technique as described in (Chattopadhyay et al, 2000). Figure 9 shows the load vs. load-line-displacement curves for various pipes. The crack grows out-of-plane in the case of carbon steel pipes. The amount of crack growth is slightly different at the two crack tips. To construct the load vs. crack growth curves and generate the component J-R curves, the average projected crack growth in the plane of the initial crack is taken. Figure 10 shows the load vs. crack growth curves for various pipes.

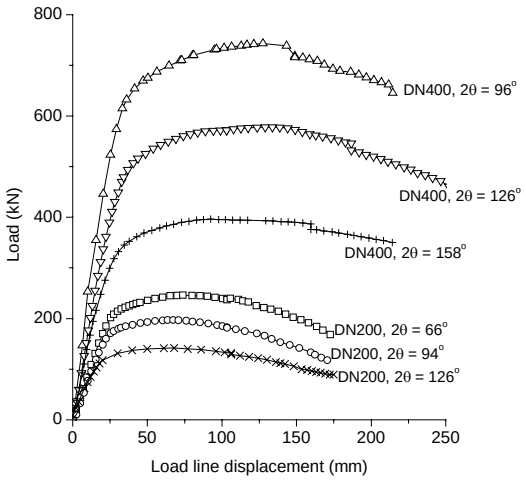

Fig. 9 Load vs. load-line-displacement curves for various through wall cracked ferritic pipes

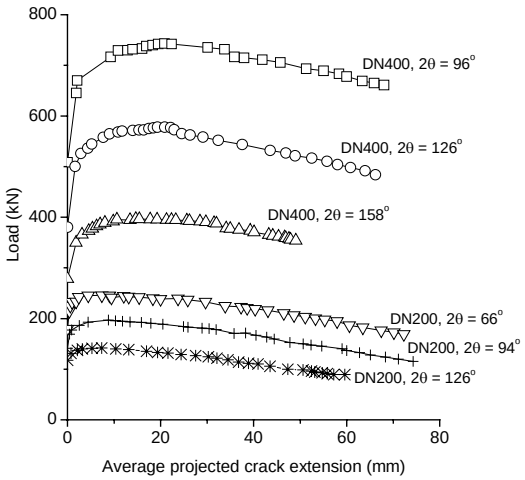

Fig. 10 Load vs. crack growth curves for various through wall cracked ferritic pipes

3.2.3 Ferritic Elbows

Figures 11 and 12 show the load vs. load-line-displacement curves for 200 and 400 mm nominal diameter elbow specimens. The figure also shows the limit loads calculated by the ASME recommended twice elastic slope method. It may be noted from Figures 11 and 12 that elbows under closing moment reached the maximum load and then the load drops after the peak value indicating instability of the structure. However, elbows under opening moment reached the maximum load asymptotically without showing any drooping behavior. This is compatible with the observations of Kussmaul et al (1995).

The crack grows out-of-plane in the case of carbon steel elbows also. The amount of crack growth is slightly different at the two crack tips. To construct the load vs. crack growth curves, the average projected crack growth in the plane of the initial crack is considered. It may be noted that crack growth, observed by the image processing technique, is on the outer surface. To get the mean value, crack growth on the outer surface has been multiplied by (R/R_o). This assumes that the crack front is radial across the thickness of the elbow. No crack growth has been observed during fracture tests of axially cracked elbows. Figures 13 and 14 show the photograph of crack growth at the end of experiment of two elbows.

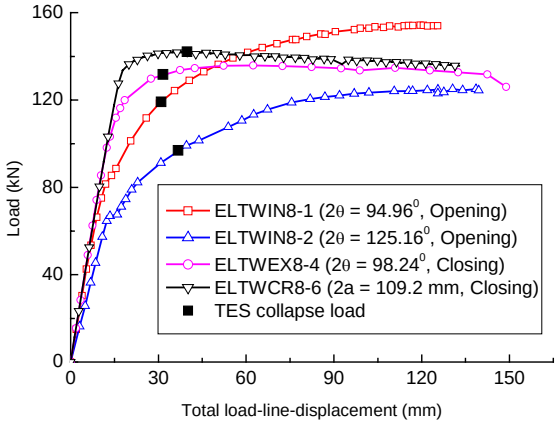

Fig.11 Experimental load-deflection curves from 200 mm NB elbows

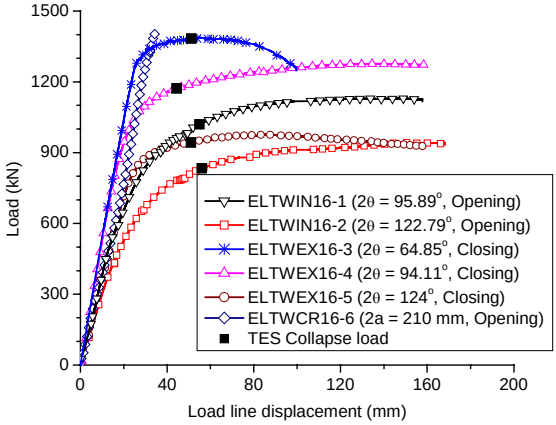

Fig.12 Experimental load-deflection curves from 400 mm nominal diameter elbows

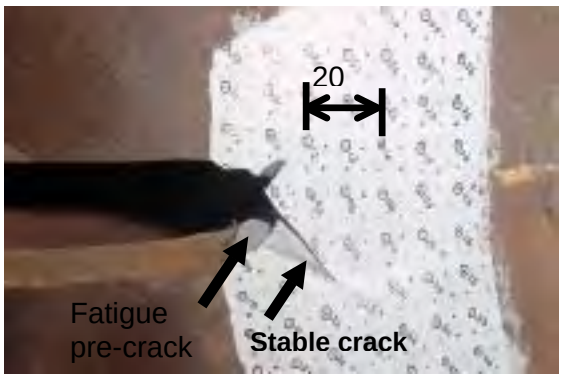

Fig.13 Crack growth at end of test of DN400 mm elbow ELTWEX16-5 (2θ=124°,Closing moment)

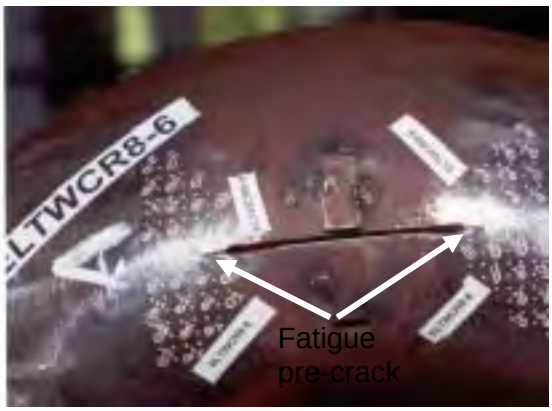

Fig.14 Crack growth at the end of experi- ment of DN200 mm through wall axially cracked elbow (Test no. ELTWCR8-6, 2a=109 mm, closing moment). No crack growth was observed.

4. COMPARISON OF EXPERIMENTAL RESULTS WITH THEORY

4.1 Austenitic Pipes

From the tests carried out at MPA Stuttgart and accessible published data, results of tests on straight pipes (nominal diameter of 50 mm to 300 mm and wall thickness from 8 mm to 30 mm) made of austenitic materials are available. In addition the failure moments have been calculated in accordance with the PLL, with the stipulation that by suitable choice of flow stress σ_f the calculated failure moment should correspond with the experimentally determined maximum moment. Figure15 shows examples for pipes of nominal diameter DN200. The good agreement of the commonly applied PLL methods with the experiments is demonstrated. To estimate the loadings (moments) at crack initiation, the R6-Method was applied to the pipe and crack geometries investigated. It turned out that independent of the pipe dimensions and crack type (surface crack or through-wall crack) the R6-Method is the most suitable for estimating the loading at crack initiation and in comparison with the test results without exception provided similar or conservative values as shown by way of example on pipes of DN200 nominal diameter in Figure 16.

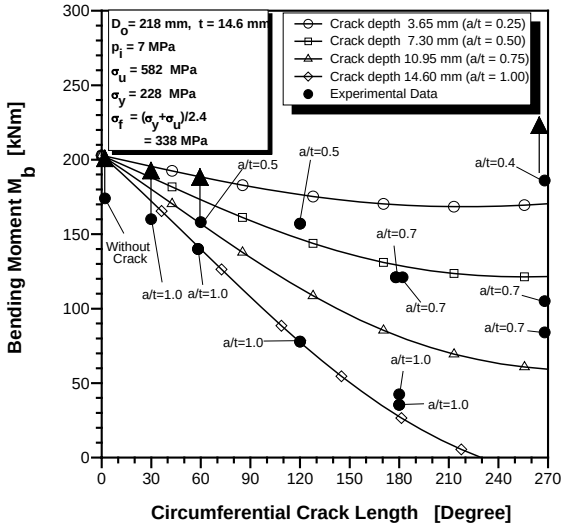

Fig.15 Failure moments as compared with experimental data for DN200 pipes calculated using the plastic limit load (PLL) concept

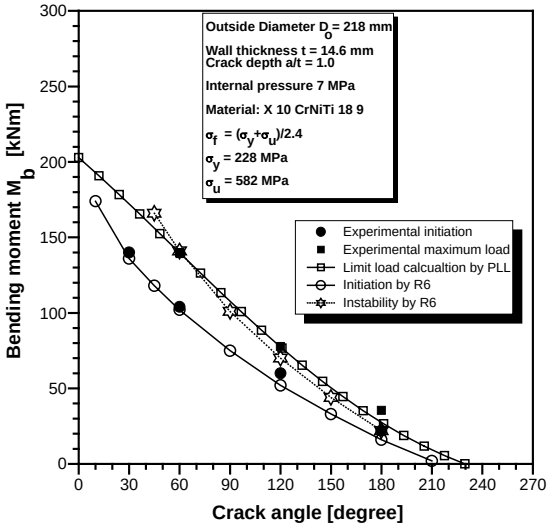

Fig.16 R6-Method and limit load calculations ($\sigma_f = [\sigma_y+\sigma_u]/2.4$) for pipes with DN200

4.2 Ferritic Pipes

In this section, limit load analyses of fracture test results of through-wall circumferentially cracked ferritic pipes are performed. The limit loads are calculated using Eqs. (1 to 3) as described in Section 2.1. Table 5 shows the comparison of the experimentally observed maximum moment with the predictions of limit moments as per Eq. (1), with $\sigma_f=\sigma_y$, $\sigma_f=(\sigma_y+\sigma_u)/2$ and $\sigma_f=(\sigma_y+\sigma_u)/2.4$. It may be seen that use of $\sigma_f=\sigma_y$ and $\sigma_f=(\sigma_y+\sigma_u)/2.4$ gave conservative results for all cases. Use of flow stress as the average of yield and ultimate stress gave quite close matching with the DN200 mm pipes. However, it gave non-conservative results in the case of DN400 mm pipes. This is because the DN200 mm pipes failed mostly in plastic collapse without much crack growth (<8 mm) until the maximum load is attained, whereas the DN400 mm pipes had stable crack growth in the range of 15 – 21 mm before the attainment of maximum load. Figure 17 shows the comparison of experimental maximum moments with the predictions as per Eq. (1) with $\sigma_f=\sigma_y$.

Table 5 Comparison of maximum experimental moments with theoretical predictions

Test specification	Initial crack angle (2θ)	Experimental max. moment (kN-m)	Predicted moments using Eq.(1) (kN-m)		
			$\sigma_f = \sigma_y$	$\sigma_f = 0.5(\sigma_y + \sigma_u)$	$\sigma_f = (\sigma_y + \sigma_u)/2.4$
DN200	66^o	155	125	153	128
DN200	94^o	124	100	123	102

DN200	126°	89	74	91	76
DN200	157°	61	51	63	53
DN400	96°	806	764	944	787
DN400	126°	627	569	703	586
DN400	158°	430	397	490	409

4.3 Ferritic Elbows

The experimentally observed twice elastic slope collapse moments are compared with the theoretical predictions by Chattopadhyay et al (2004) through Eqs. (7-10), Miller (1988) through Eqs. (5,6) and Zahoor (1990) through Eqs. (4, 5 and 11). The weakening factors (M_L/M_0) for closing bending using the Eqs. (7 and 8) proposed by Chattopadhyay et al (2004) for intermediate R/t have been linearly interpolated between two adjacent R/t values. To get the corresponding moment from the experimental load, load is multiplied by the perpendicular distance between the load line and middle of elbow axis which are shown in Table 4. Although this distance changes during loading of the elbow, the change has been found to be negligible compared to the initial distance and hence has not been accounted for in the calculation. In terms of applicability

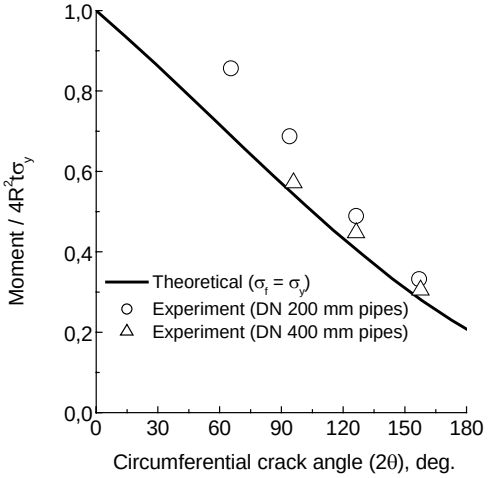

Fig.17 Comparison of theoret. limit moment (init. crack angle) with exp. maximum moment

of Eqs. (4 and 5) and (11), although the limits of elbow factor ($h=4R_bt/D^2 \leq 0.5$) and crack length ($a/D<0.8$ or 0.9) are satisfied, the condition of $D/t \geq 15$ is violated here. The flow stress of the material required as input in both Miller's and Zahoor's equations (Eq. 5) is defined as the average of yield and ultimate strength, which are shown in Table 2. Table 6 shows the comparison of theoretical and experimental moment values. It may be seen that the predictions by Miller (1988) is too conservative. The prediction of Chattopadhyay et al (2004) is quite close to the test results. The prediction of Zahoor (1990) was not consistent with respect to conservatism and not so accurate also.

5. CONCLUSIONS

Fracture tests on cracked austenitic and ferritic pipes and elbows of sizes ranging from nominal diameter 50 to 400 mm have been carried out. The test results have been analysed and compared with the theoretical predictions by plastic limit load and R6 approaches. From these analyses, it is recommended for safe assessment of pipes within the dimensions and materials covered in this study to use the plastic limit load concept using $\sigma_f=(\sigma_y+\sigma_u)/2.4$ and for other cases to use $\sigma_f=\sigma_y$. For through-wall circumferentially cracked elbows, it is recommended to use the limit load Eqs. (7-10) recently proposed by Chattopadhyay et al (2004). It is also seen from this study that the R6 method is quite accurate in prediction of crack initiation loads.

Table 6 Comparison of experimental twice elastic slope collapse moments with predictions (the brackets indicate the percent. difference with respect to experimental values)

Test no.	Experimental collapse moment (kN-m)	Predicted Collapse moment (kN-m)		
		Chattopadhyay et al (2004), Eqs.(7-10)	Miller (1988), Eqs.(5,6)	Zahoor (1990), Eqs.(4,5,11)
ELTWIN8-1	98.4	101.1 (-2.7%)*	82.3 (16.4%)	112.8 (-14.6%)

ELTWIN8-2	80.0	76.0 (5%)	63.6 (20.5%)	92.65 (-15.8%)
ELTWEX8-4	108.7	100.2 (7.8%)	82 (24.6%)	113.2 (-4.1%)
ELTWEX8-6	117.2	-	-	129.5 (-10.5%)
ELTWIN16-1	857.0	847.1 (1.2%)	807.9 (5.7%)	1109.6 (-29.5%)
ELTWIN16-2	699.1	678.8 (2.9%)	669.2 (4.3%)	971.8 (-39%)
ELTWEX16-3	1161.2	1092.3 (5.9%)	923.4 (20.5%)	1153.6 (0.7%)
ELTWEX16-4	985.6	962.1 (2.4%)	792.5 (19.6%)	1083.3 (-9.9%)
ELTWEX16-5	792.3	819.4 (-3.4%)	682.8 (13.8%)	993.1 (-25.3%)
ELTWCR16-6	> test range	-	-	-

* % difference = [(experim. – predicted) /experim.] × 100%

REFERENCES

ASME Boiler and Pressure Vessel Code, Sec.III, (**2001**), American Society of Mechanical Engineers

J.Chattopadhyay, B.K.Dutta and H.S.Kushwaha, (**2000**), "Experimental and analytical study of three point bend specimens and through wall circumferentially cracked straight pipe", *International Journal of Pressure Vessels and Piping* **77**, pp 455 – 471

J.Chattopadhyay, A.K.S.Tomar, B.K:Dutta and H.S.Kushwaha, (**2004**), "Closed-form collapse moment equations of through wall circumferentially cracked elbows subjected to in-plane bending moment", *Journal of Pressure Vessel Technology*, ASME Transactions **126**, pp 307 – 317

J.Chattopadhyay, T.V.Pavankumar, B.K.Dutta and H.S.Kushwaha, (**2005**), "Fracture experiments on throughwall cracked elbows under in-plane bending moments : Test results and theoretical/numerical analyses", *Engineering Fracture Mechanics* , (in press)

M.F.Kanninen, A.Zahoor, G.M.Wilkowski, I.Abousayed, C.Marschall, D.Broek, S.Sampath, H.Rhee and J.Ahmad, (**1982**), "Instability Predictions for Circumferentially Cracked Type 304 Stainless Steel Pipes Under Dynamic Loading", EPRI-NP-2347, Vol.1 & 2, Electric Power Research Institute, Palo Alto, CA

W.Kastner, E.Rohrich, W.Schmitt and R.Steinbuch, (**1981**), "Critical Crack Sizes in Ductile Piping", *Int. Journal of Pressure Vessel and Piping* **9**, pp 197 – 219

K.Kussmaul, H.K.Diem, D.Uhlmann and E.Kobes, (**1995**), "Pipe Bend Behaviour at Load Levels Beyond Design" Proceedings of 13th International Conference on Structural Mechanics in Reactor Technology, SMiRT. Brazil, **G**, pp 187-198.

A.G.Miller, (**1988**), "Review of Limit Loads of Structures Containing Defects", *Int. J. of Pres. Ves. and Piping* **32**, pp 197 – 327.

I.Milne, R.A. Ainsworth, A.R. Dowling and A.T. Stewart; "Assessment of the integrity of structures containing defects". *R/H/R6 - Rev. 3*, Central Electricity Generating Board, May, **1986**

D.Moulin and P.Delliou, (**1996**), "French Experimental Studies of Circumferentially Through-Wall Cracked Austenitic Pipes under Static Bending", *Int. J. of Pressure Vessel and Piping* **65**, pp 343 - 352

E.Roos, K.-H.Herter and F.Ottremba, (**2000**), "Testing of Pressure Vessels, Piping and Tubing", ASM Handbook, Vol.8, Mechanical Testing and Evaluation, Oct., pp 873 - 885

A.Zahoor, (**1990**), Ductile Fracture Handbook, Vol.3